Research Article | Vol. 30, No. 9 / 25 Apr 2022 / Optics Express 14061
Optics EXPRESS

Enhancing critical resolution of a ghost imaging system by using a vortex beam

WEI TAN,[1] YANFENG BAI,[1,3] XIANWEI HUANG,[1] TENG JIANG,[1] SUQIN NAN,[2] QIN FU,[1] XUANPENGFAN ZOU,[1] AND XIQUAN FU[1,4]

[1]College of Computer Science and Electronic Engineering, Hunan University, Changsha 410082, China
[2]School of Computer Science, Hunan University of Technology and Business, Changsha 410205, China
[3]yfbai@hnu.edu.cn
[4]fuxq@hnu.edu.cn

Abstract: In an imaging system, resolution and signal-to-noise ratio (SNR) are two important indexes to characterize imaging quality. Ghost imaging is a novel imaging method whose imaging resolution and SNR are affected by the speckle size. In this paper, the relation between speckle size and resolution as well as that between speckle size and SNR in the GI system is analyzed in detail. It is shown that the critical resolution, resolvable minimum-separation between two adjacent objects, is approximately equal to the speckle size (speckle diameter). There exists an optimum SNR when the speckle size is larger than the object size. Based on our conclusion, we propose a scheme to enhance the critical resolution of the GI system by using a vortex beam, and the enhancement ability under different topological charges is clearly presented, which can be quantized by a simple formula.

1. Introduction

Different from conventional imaging technique, ghost imaging (GI), a non-local imaging technique, retrieves the image of an object by intensity correlation measurements between two spatial separated light beams. It was first experimentally verified in 1995 by using entangled photon pairs [1], making many thought that GI was a pure quantum phenomenon. In 2002, Bennink *et al*. experimentally presented a contrary evidence that GI with a classical source can also be achieved [2]. Subsequently, many GI experiments with classical sources have been reported successively, including true thermal light [3] and pseudo-thermal light [4]. Since then, GI with pseudo-thermal light has been received considerable attentions owing to its convenience configurations, and significant progress has been made in medical imaging [5], military detection [6], lidar [7] and remote sensing [8]. However, its imaging signal-to-noise ratio (SNR) is usually inferior to conventional imaging because of the nature of statistical correlation. For this reason, many algorithms have been developed to enhance imaging SNR of GI, such as compressive sensing [9], differential operation [10], and pseudo-inverse operation [11]. Especially in recent years, GI has been benefited widely by the advances in deep learning-based algorithms [12,13].

For any imaging system, an image with high resolution and SNR is pursuant for high-quality imaging. In conventional imaging system, the imaging SNR is equal to the system's detection SNR [14]. The spatial resolution is determined by the point spread function (PSF) of the system [15] and the resolution limit is usually given by the Rayleigh diffraction limit [16], which is defined as the resolvable minimum-separation between two points [17,18]. In GI system, these factors that affect imaging quality are quite complex because of its statistical characteristics. The influence from speckle field characteristics (e.g., statistical distribution and size) on imaging quality has become a research hotspot in recent years [19–27]. It is shown that by changing the statistical distribution of speckle fields, e.g., non-negative exponential [25] and sub-Rayleigh

#455399 https://doi.org/10.1364/OE.455399
Journal © 2022 Received 1 Feb 2022; revised 11 Mar 2022; accepted 28 Mar 2022; published 11 Apr 2022

Optics EXPRESS

speckle fields [26], the imaging resolution can be improved. An increase of the speckle size can improve the SNR of reconstructed images [19–24,27], but reduce the resolution. In other words, decreasing the speckle size results in higher resolution at the expense of a reduced SNR. Hence, it is very important to choose an appropriate speckle size to tradeoff between resolution and SNR for high-quality GI.

In this paper, the influence of the speckle size on the resolution and SNR in GI system is investigated experimentally and numerically. The speckle size is controlled by imaging distance, and it is shown that the resolution of GI reaches the limit, which is the minimum resolution for distinguishing two adjacent objects when the speckle size (speckle diameter) is approximately equal to the separation of two objects. In other words, the critical resolution [28], resolvable minimum-separation between two adjacent objects, is approximately equal to the speckle size. In addition, an optimum SNR can be obtained by adjusting the speckle size when the speckle size is larger than the object size. The numerical and experimental results verify our conclusion. To improve the critical resolution, a GI scheme by using a vortex beam instead of the Gaussian beam is proposed, and the results show that increasing the topological charge of the vortex beam can result in smaller speckle size, thus obtain higher critical resolution. Moreover, we provide an analytical formula to quantify the enhancement ability under different topological charges, and the formula of critical resolution in GI system with the vortex beam is also given.

2. Model and theory

2.1. Measurement of the statistical size of speckle patterns

The experimental setup to measure the statistical size of speckle patterns is shown in Fig. 1(a). A collimated laser beam after passing through the phase modulator (PM) is used to irradiate the rotating ground-glass (RGG) to generate speckle patterns, which are recorded by a charge-coupled device (CCD). According to speckle statistics theory [29], one can obtain the statistical size of the speckle pattern by autocorrelation operation. In our numerical model, the modulation effect of ground-glass on the incident beam can be expressed using a transmission matrix T with circular Gaussian distribution, which is shown in Fig. 1(b). Thus, we have

$$E_{\text{out}} = E_{\text{in}} \cdot T, \tag{1}$$

where E_{in} (E_{out}) is the field distribution on the front (rear) surface of the ground glass.

Through the Fresnel diffraction integral, we can deduce the intensity distribution expression of the speckle field at z distance after the beam passing through the ground glass.

$$I(x,y,z) = \left| \frac{\exp(ikz)}{i\lambda z} \int_{-\infty}^{+\infty} \int_{-\infty}^{+\infty} E_{\text{out}}(\xi,\eta,0) \cdot \exp\left\{ \frac{ik}{2z}[(x-\xi)^2 + (y-\eta)^2] \right\} d\xi d\eta \right|^2, \tag{2}$$

where (ξ,η,0) is the coordinates of the plane where the ground glass is located, and (x,y,0) is the coordinates of the observation plane. Similarly, carrying out the autocorrelation operation on the speckle pattern obtained by Eq. (2), we can acquire the statistical size of the speckle pattern.

Assuming the output beam modulated by PM is a Laguerre-Gaussian vortex beam, the beam profile in the cylindrical coordinates system can be written as [30]:

$$E^l(\rho,\theta,z=-p) \propto \left(\frac{\rho}{W_0}\right)^{|l|} \exp\left(-\frac{\rho^2}{{W_0}^2}\right) \exp(il\theta), \tag{3}$$

where p is the distance from the PM to the RGG. W_0 and l are the beam waist radius and topological charge, respectively. According to the Collins diffraction integration formula [31],

Optics EXPRESS

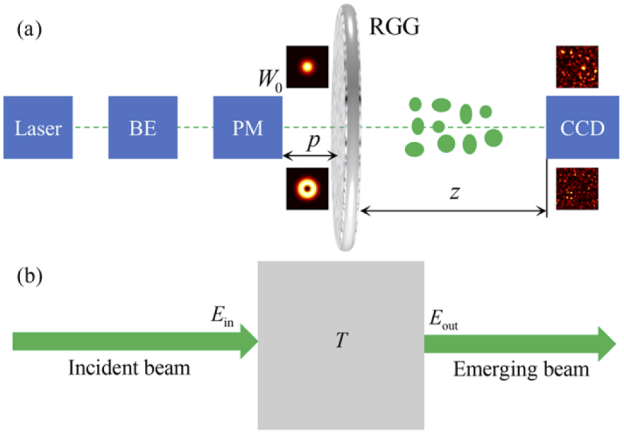

Fig. 1. (a) Experimental setup for a measurement of the statistical size of speckle patterns. BE: beam expander; PM: phase modulator; RGG: rotating ground-glass; CCD: charge-coupled device. W_0 represents the waist radius after the laser beam passes through the BE and z is the distance from the RGG to the CCD. (b) Schematic diagram of beam propagating through a ground glass.

the light field on the front surface of RGG can be expressed as

$$E^l(\rho,\theta,z=0) \propto \left(\frac{W_0}{W_p}\right)\left(\frac{\rho}{W_p}\right)^{|l|} \exp\left(-\frac{\rho^2}{{W_p}^2}\right) exp\left(\mathrm{i}\,|l|\,\theta\right) \exp\left(\mathrm{i}kp + \mathrm{i}\frac{2p}{k{W_0}^2}\frac{\rho^2}{{W_p}^2}\right), \quad (4)$$

where k is the wave number, $W_p = W_0\sqrt{(1+p^2/{z_R}^2)}$, $z_R = k{W_0}^2/2$. In our experiment, $p \ll z_R$, so$W_p \approx W_0$. Note that when $l=0$, the vortex beam degenerates into a typical Gaussian beam, which can be viewed as a special case of vortex beam. According to Ref. [32], the theoretical formula for the statistical size (speckle statistical diameter) of speckle patterns generated by a Gaussian beam is given by

$$S = \frac{2\lambda z}{\pi W_0}, \quad (5)$$

where z is the distance after a Gaussian beam passing through a RGG. Based on the above theoretical analysis, we set $W_0 = 1$ mm, the speckle size S under different topological charge l versus propagation distance z is shown in Fig. 2(a).

For the Gaussian beam ($l=0$), one can find that the simulation and experimental values match well with theoretical results, which confirms the reliability of our numerical model and experimental measurement. For the vortex beam ($l \neq 0$), the simulation values match well with experimental results. In addition, one can clearly see that the speckle sizes from the vortex beam are smaller than those of the Gaussian beam under the same propagation distance, and the larger the topological charge is, the smaller speckle size is. At the same time, Fig. 2(b) shows the speckle patterns when the topological charge l chooses different values under propagation distance $z=0.5$ m, which intuitively shows the changing trend of the speckle size.

2.2. Experimental description of GI and imaging quality assessment

The experimental setup of GI with the vortex beam is schematically illustrated in Fig. 3. A fundamental Gaussian beam is generated by a CW single-frequency laser at 532 nm. The first circular aperture (CA1) and laser attenuator (LA) are used to filter out the stray light and adjust the intensity of the beam, respectively. The variable beam expander (VBE) is used to collimate

Optics EXPRESS

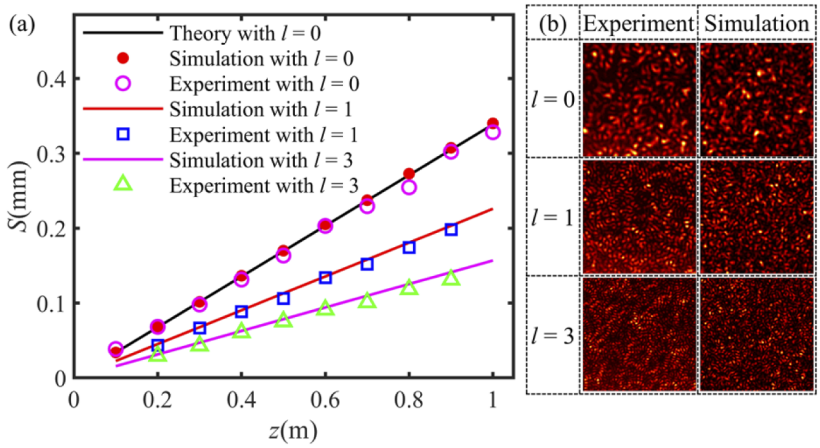

Fig. 2. (a) Speckle size S as a function of the propagation distance z under different topological charge l. (b) The speckle patterns versus topological charge under propagation distance $z = 0.5$ m.

and expand the beam, and the second circular aperture (CA2) is used to modulated the diameter of output beam. The first laser polarizer (LP1) is used to control the direction of polarization of the laser beam, allowing the spatial light modulator (SLM) to achieve maximum modulation. The prescribed phase picture is loaded onto the SLM, which can generate the Laguerre-Gaussian vortex beam. The second laser polarizer (LA2) behind the SLM is used as a polarization analyzer to filter out the stray light, and the third circular aperture (CA3) is used to eliminate conjugate image of the vortex beam made by the SLM. Then the speckle source, generated by the vortex beam illuminating the slowly RGG, is divided by using a beam splitter (BS) into the reference and object beams. In the reference path, the intensity distribution of the speckle field is detected by a CCD camera (Thorlabs DCC3240C: 1024×1280 pixels, pixel size: 5.3 µm). In the object path, the speckle field passes through a transmissive object, and then all transmitted photons are collected by a bucket detector (Thorlabs PDA100A2: the detected aera 75.4 mm^2, the gain range: 0-70 dB).

According to the classical GI theory, we can obtain the object information $G(\rho)$ using the following correlation function [33,34]

$$G(\rho) = \frac{1}{N}\sum_{n=1}^{N} I_r^n(\rho) I_b^n - \frac{1}{N}\sum_{n=1}^{N} I_r^n(\rho)\frac{1}{N}\sum_{n=1}^{N} I_b^n, \tag{6}$$

where $I_b^n = \sum_{\rho} I_r^n(\rho)T(\rho)$,$I_r^n(\rho)$, $T(\rho)$ and N are the total signal of the bucket detector for the nth measurement, the intensity of the projected field at location ρ recorded by the CCD camera for the nth measurement, the transmission function of the object and the total number of measurements, respectively. For simplicity, it is assumed that the object has binary transmission. i.e., the value of $T(\rho)$ is either zero or unity. In order to quantitatively analyze imaging quality, the SNR is generally used, which is defined as [35]

$$\mathrm{SNR} = \frac{\langle I_S\rangle - \langle I_N\rangle}{\sqrt{\frac{1}{2}(V_S + V_N)}}, \tag{7}$$

where $\langle I_S\rangle$ and $\langle I_N\rangle$ are the ensemble average of the reconstructed object signal with the transmission being one and zero, respectively. V_S and V_N are the corresponding variances, respectively.

Optics EXPRESS

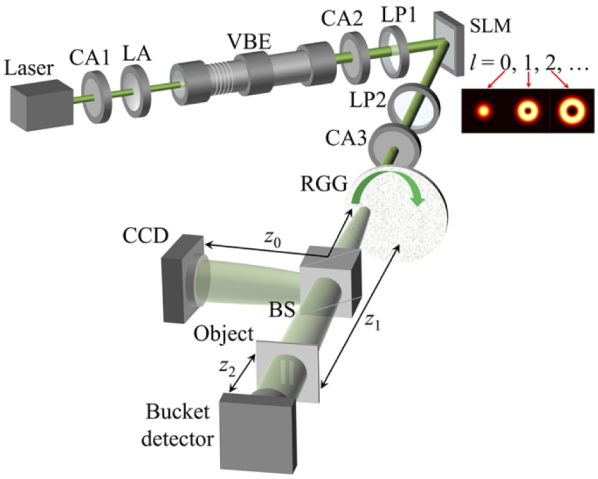

Fig. 3. Schematic diagram of experimental setup for GI with the vortex beam. CA1, CA2, CA3: circular apertures; LA: laser attenuator; LP1, LP2: laser polarizers; VBE: variable beam expander; SLM: spatial light modulator; BS: beam splitter. l is the topological charge of generated vortex beam. z_0, z_1 and z_2 are the distances from the RGG to the CCD, from the RGG to the object, and from the object to the bucket detector, respectively.

The evaluating method of the spatial resolution of the reconstructed image is shown in Fig. 4. Here, the white square with a side of length h (double-slit height) is chosen as an area covering signal and background to calculate the resolution. The R value, which is defined as the ratio of the intensity at the ghost-image center to the maximum intensity [36], is chosen as the evaluation criterion of imaging resolution. It is worth mentioning that the average value of the pixel values in the y direction is used to replace the pixel value at $y = 0$ to degrade the impact of noise. Thus,

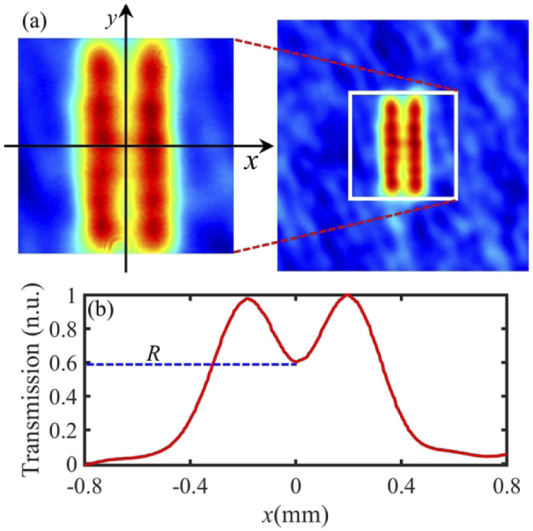

Fig. 4. Method of resolution measurement of a retrieved image.

Optics EXPRESS

R can be expressed as

$$R = \frac{\frac{1}{M}\sum_{j=1}^{M} G(x=0,y_j) - \left[\frac{1}{M}\sum_{j=1}^{M} G(x,y_j)\right]_{\min}}{\left[\frac{1}{M}\sum_{j=1}^{M} G(x,y_j)\right]_{\max} - \left[\frac{1}{M}\sum_{j=1}^{M} G(x,y_j)\right]_{\min}}, \tag{8}$$

where M represent the pixel numbers in the y direction. The smaller the R value is, the higher the resolution of the reconstructed image is, which is indicated by a blue dashed line in Fig. 4(b).

3. Experimental and simulation results

In our experiments, the imaging object is chosen as a double-slit, whose center-to-center separation d is twice slit width w, i.e., $d = 2w$. The exposure time of the CCD is 0.25 ms, the gain of the bucket detector is 70 dB, the number of measurements is 10000 and the imaging distances shown in Fig. 3 satisfy: $z_0 = z_1$. In our simulations, the sampling points is 480×480, and other parameters are identical to those in the experiments.

3.1. Exploring the critical resolution and optimum SNR of the GI system

We consider the speckle field generated by Gaussian beam ($l = 0$ in Eq. (4)), and the effects of speckle size on GI are examined. From Eq. (3), different speckle sizes S can be obtained by changing the imaging distance z_0 or adjusting the beam width W_0. Here, we set $d = 0.4$ mm, $W_0 = 1$ mm, and z_0 is increased from 0.295 m to 1.772 m in 6 steps. The experimental and simulation results are shown in Fig. 5. It is obvious that the speckle size gradually increases for lager imaging distance in Figs. 5(a) and (c), here S of every speckle pattern is marked at the bottom. The reconstructed ghost-images are given in Figs. 5(b) and (d). As the imaging distance increases, i.e., the increment of the speckle size, the back noise of the ghost images become lower and lower, while the resolution of ghost-images is degraded and finally the two slits cannot be distinguished. For quantitatively depicting the change of the resolution, R is presented in Figs. 5(e). With the increase of the imaging distance, the value of R keeps increasing, which means that the imaging resolution is getting lower and lower. In addition, it is worth noting that the image of the double slit is barely distinguishable when the imaging distance is 1.181 m [see Figs. 5(b4) and (d4)], which corresponds to the speckle size being about 0.4 mm. Based on the Rayleigh criterion, the value of R is 0.81 [18] when two rectangular apertures are just distinguishable. As can be seen from Fig. 5(e), the value of R is about 0.81 when the imaging distance is 1.181 m ($S \approx 0.4$ mm) both in experiment and simulation. i.e., the critical resolution (the resolvable minimum-separation between two adjacent objects), denoted d_R, appears when the speckle size is about the slit separation ($d = 0.4$ mm), which is of great significance to evaluate the imaging capability of GI system. In addition, the function relationship between SNR of ghost-images and imaging distance z_0 or speckle size S is plotted in Fig. 5(f). One can find that the laws of SNR versus the speckle size S is different from the previous works [19–24,27], i.e., the value of SNR increases first and then decreases with the increase of the speckle size S, while the SNR increases monotonically as S increases in previous works. In fact, our result does not conflict with that in previous works. The previous works only considered the case where the speckle size S is smaller than the object size w. When $S < w$, the double-slit is clearly distinguishable. Under the circumstances, the SNR of ghost-image is mainly affected by the background noise [see Figs. 5(b1) and (d1)], so the SNR increases monotonously with the increase of the speckle size. When $S > w$, as the speckle size increases, the resolution of ghost-image becomes lower and lower, resulting in blurred and widened double-slit. In the process of calculating of the SNR [see Eq. (7)], the widened region of the double-slit is treated as the noise. When the increment of

Optics EXPRESS

this noise is greater than the decrement of background noise, the SNR of ghost-image is mainly affected by this noise, which leads to the decrease of SNR.

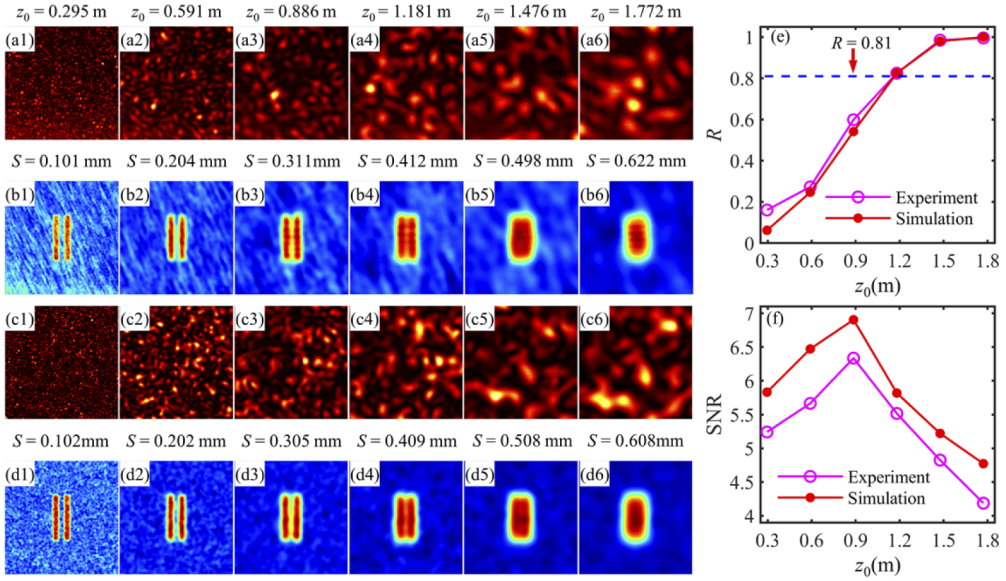

Fig. 5. The speckle patterns and reconstructed ghost-images versus speckle size S controlled by imaging distance z. (a), (b) Experimental results. (c), (d) Simulation results. (e), (f) The dependences of the R and the SNR on the imaging distance.

3.2. *Verificating the critical resolution and optimum SNR of the GI system*

Based on the discussion in Section 3.1, two important conclusions can be drawn: (1) the critical resolution d_R of GI system is approximately equal to the speckle size S under $d = 2w$, i.e., $d_R \approx S$; (2) GI system exists a maximum of SNR for a given object size, which can be achieved by adjusting the speckle size. To prove that the above conclusions are general, we consider some other cases in the hope of reaching the same conclusions.

Firstly, we set the slit separation $d = 0.2$, 0.3, 0.5 and 0.6 mm, and the corresponding speckle sizes are about 0.2, 0.3, 0.5 and 0.6 mm, respectively to demonstrate the critical resolution of GI system. Figure 6(a) shows the experimental results of the reconstructed ghost-images and the corresponding simulation results are presented in Fig. 6(b). The two slits of ghost-images which are visible to the naked eye are in the state that is just distinguishable. Further, the R value of ghost-images for different d is plotted in Fig. 6(c), here the theoretical R value of critical resolution is indicated by a blue dashed line. One can find that although some of the results are slightly different from the theoretical value, the error of experimental and simulation results is lower than 2.23%. Therefore, the experimental and simulation results match well with the theoretical value 0.81, which confirms the reliability of our conclusion (1). Thus, the critical resolution of pseudo-thermal GI system under $d = 2w$ can be express as:

$$d_R \approx \frac{2\lambda z}{\pi W_0}. \tag{9}$$

Next, we further demonstrate the laws of SNR versus the speckle size S shown in Fig. 6(d) under different object sizes ($w = 0.25$ and 0.3 mm). Obviously, the optimum SNR appears when $S > w$, which confirms the reliability of our conclusion (2).

Optics EXPRESS

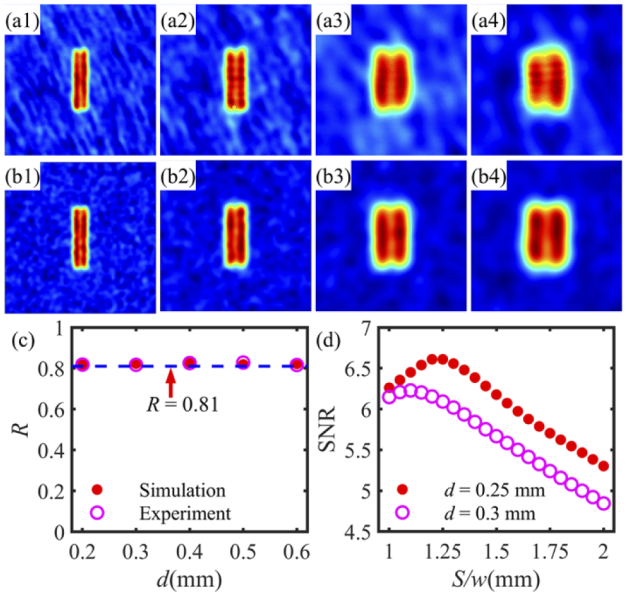

Fig. 6. (a) and (b) are the experimental and simulation results when the slit separation d is comparable to the speckle size S, respectively. (c) is the R versus d. (d) is the SNR versus S/w.

3.3. *Enhancing critical resolution of the GI system by using a vortex beam*

According to the above analysis, the critical resolution of pseudo-thermal GI system is determined by the speckle size, and the critical resolution is approximately equal to the speckle size, which means that the critical resolution can be enhanced by decreasing the speckle size. In Section 2.1, we have presented the comparison between the propagation effect for the Gaussian beam and vortex beam, which clearly shows that the speckle sizes from the vortex beam are smaller than those of the Gaussian beam under the same propagation distance. Based on these conclusions, we propose a scheme to enhance the critical resolution in GI system by replacing the Gaussian beam with the vortex beam.

Firstly, we consider the slit separation $d = 0.4$ mm and the imaging distance $z_0 = 0.886$ m to demonstrate the resolution enhancement of GI system by using vortex beam. Figure 7 shows the ghost-images obtained under different topological charges. Figures 7(a) and (b) are the experimental and simulation results, respectively. Although the two slits of ghost-images from Gaussian beam ($l = 0$) can be distinguished, the resolution is low. Compared with the Gaussian beam, the two slits of ghost-images from vortex beam ($l = 1$ and 3) can be clearly distinguished, and the larger the topological charge, the better the discrimination effect, which means that the resolution of ghost-images is improved by using vortex beam, and the greater the topological charge, the better the improvement.

Next, we discuss the improvement effect of vortex beam on the critical resolution of GI system. The reconstructed ghost-images versus imaging distance under different topological charges are shown in Figs. 8(a)-(d), here the slit separation is $d = 0.2$ mm. The first and second rows are the experimental and simulation results, respectively. For the convenience of comparison, Figs. 6(a1) and (b1) are redrawn in Fig. 8(a). When the imaging distance is equal to 0.591 m, the two slits of ghost-images from the Gaussian beam ($l = 0$) are just distinguishable, which means that the critical resolution d_R is about 0.2 mm [see Fig. 8(a)]. While the double-slit pattern by using the vortex beam ($l = 1$) can be clearly distinguished, indicating that the critical resolution is

Optics EXPRESS

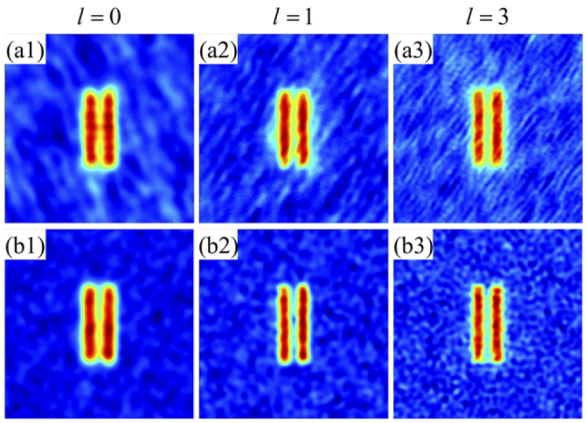

Fig. 7. The reconstructed ghost-images versus topological charge under slit separation $d = 0.4$ mm. (a) Experimental results. (b) Simulation results.

improved [see Figs. 8(b)]. This fact can also be demonstrated from the evolution of R, and the corresponding R values of the experimental and simulation results increase by 35.85% and 50%, respectively when the vortex beam is considered. For the longer imaging distance ($z_0 = 0.886$ m), the double-slit pattern is barely distinguishable in Fig. 8(c) under the topological charge $l = 1$, while the two slits can be clearly distinguished as shown in Fig. 8(d) for the higher topological charge ($l = 3$), and the R value in the experimental and simulation results increase by 24.15% and 41.63%, respectively. Therefore, one can conclude that the critical resolution of GI can be significantly improved by using the vortex beam when compared with that with the Gaussian beam. At the same time, GI with longer imaging distance can be achieved by increasing the topological charge number of the vortex beam under the same critical resolution, as shown in Fig. 8(e). The above results can be explained by the change of the speckle size plotted in Fig. 8(f). One can clearly see that the speckle sizes from the vortex beams are smaller than those of the Gaussian beam, and the speckle size decreases with increasing the topological charge number of the vortex beam, thus a larger critical resolution can be obtained.

To quality the above result, we choose Q_l to represent the enhancement ability of critical resolution by replacing the Gaussian beam with the vortex beam, and $Q_l = S_G/S_V$. Here, S_G and S_V are the speckle size generated by the Gaussian beam and vortex beam, respectively. The function relationship between Q_l and l is plotted in Fig. 9(a). Obviously, Q_l gradually increases for larger l, i.e., the larger the topological charge is, the stronger the enhancement ability. At the same time, a fitting function $Q_l = \mathrm{A}l^{\mathrm{B}} + \mathrm{C}$ is performed to formalize the relationship between the enhancement ability and the topological charge. The fitted curve (solid line) match well with the simulation data (open circles). Thus, the critical resolution in GI system with the vortex beam can be expressed as :

$$d_R \approx \frac{2\lambda z}{\pi Q_l W_0}, \tag{10}$$

where $Q_l = 0.9788l^{0.5214} + 0.4740$ and $l \geq 1$. Morever, the comparison between the critical resolution with the vortex beam and the Rayleigh diffraction limit ($0.61\lambda z/W_0$) is presented, as shown in Fig. 9(b). Obviously, the critical resolution with the vortex beam (l>0) can exceed the Rayleigh diffraction limit.

Optics EXPRESS

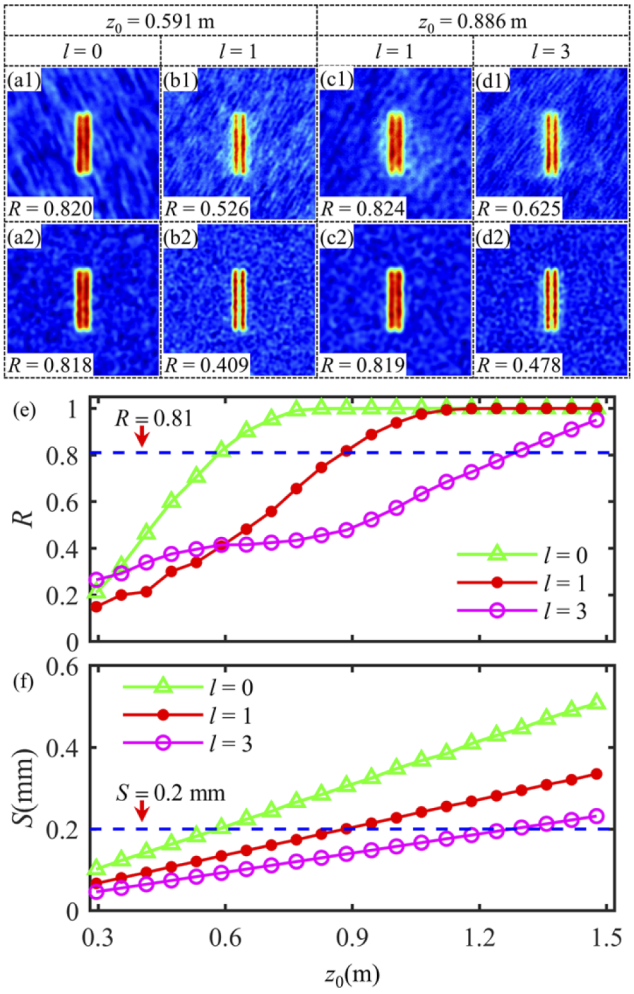

Fig. 8. The reconstructed ghost-images versus imaging distance with slit separation $d = 0.2$ mm under different topological charges. (a) $z_0 = 0.591$ m, $l = 0$; (b) $z_0 = 0.591$ m, $l = 1$; (c) $z_0 = 0.886$ m, $l = 1$; (d) $z_0 = 0.886$ m, $l = 3$. The first and second rows are the experimental and simulation results, respectively. (e), (f) The dependence of R and S on the imaging distance, respectively.

Optics EXPRESS

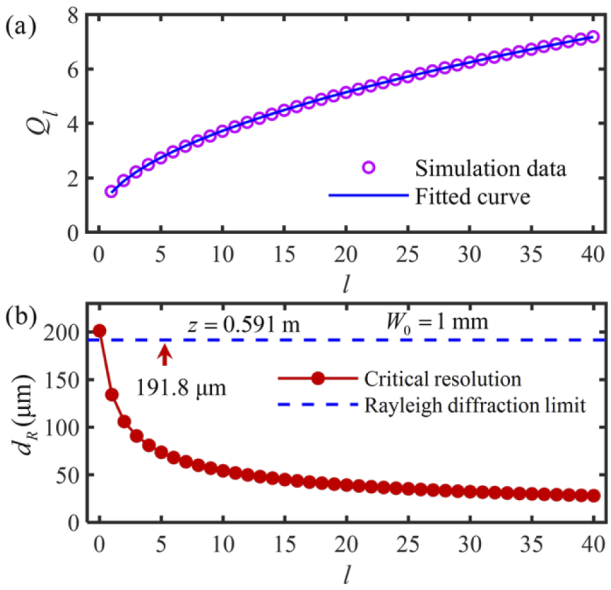

Fig. 9. (a) and (b) are the dependences of the enhancement ability Q_l and critical resolution d_R on the topological charge l, respectively.

4. Conclusions

In conclusion, we have experimentally and numerically investigated the effects of the speckle size (speckle diameter) controlled by the imaging distance on resolution and SNR of GI. It is shown that the critical resolution (the resolvable minimum-separation d_R between two adjacent objects) of GI system is approximately equal to the speckle size and an optimum SNR exists in GI system, which is verified by the corresponding experimental and simulation results. In addition, the scheme of improving the critical resolution of GI system is proposed by using the vortex beam, and the results show that the critical resolution can be significantly enhanced by replacing the Gaussian beam with the vortex beam. Moreover, a quantitative formula about the critical resolution of GI system with vortex beam is given, which can be useful for designing GI system and remote sensing.

Funding. National Natural Science Foundation of China (61871431, 61971184, 62001162, 62101187).

Disclosures. The authors declare no conflicts of interest.

Data availability. Data underlying the results presented in this paper are not publicly available at this time but may be obtained from the authors upon reasonable request.

References

1. T. B. Pittman, Y. H. Shih, D. V. Strekalov, and A. V. Sergienko, "Optical imaging by means of two-photon quantum entanglement," Phys. Rev. A **52**(5), R3429–R3432 (1995).
2. R. S. Bennink, S. J. Bentley, and R. W. Boyd, "Two-photon coincidence imaging with a classical source," Phys. Rev. Lett. **89**(11), 113601 (2002).
3. Y. H. Zhai, X. H. Chen, D. Zhang, and L. A. Wu, "Two-photon interference with true thermal light," Phys. Rev. A **72**(4), 043805 (2005).
4. J. Xiong, D. Z. Cao, F. Huang, H. G. Li, X. J. Sun, and K. Wang, "Experimental observation of classical subwavelength interference with a pseudothermal light source," Phys. Rev. Lett. **94**(17), 173601 (2005).
5. D. Pelliccia, A. Rack, M. Scheel, V. Cantelli, and D. M. Paganin, "Experimental X-Ray ghost imaging," Phys. Rev. Lett. **117**(11), 113902 (2016).
6. H. C. Liu and S. Zhang, "Computational ghost imaging of hot objects in long-wave infrared range," Appl. Phys. Lett. **111**(3), 031110 (2017).
7. B. I. Erkmen, "Computational ghost imaging for remote sensing," J. Opt. Soc. Am. A **29**(5), 782–789 (2012).

Optics EXPRESS

8. C. Q. Zhao, W. L. Gong, M. L. Chen, E. R. Li, H. Wang, W. X. Xu, and S. S. Han, "Ghost imaging lidar via sparsity constraints," Appl. Phys. Lett. **101**(14), 141123 (2012).
9. O. Katz, Y. Bromberg, and Y. Silberberg, "Compressive ghost imaging," Appl. Phys. Lett. **95**(13), 131110 (2009).
10. F. Ferri, D. Magatti, L. A. Lugiato, and A. Gatti, "Differential ghost imaging," Phys. Rev. Lett. **104**(25), 253603 (2010).
11. C. Zhang, S. Guo, J. Cao, J. Guan, and F. Gao, "Object reconstitution using pseudo-inverse for ghost imaging," Opt. Express **22**(24), 30063–30073 (2014).
12. M. Lyu, W. Wang, H. Wang, H. C. Wang, G. W. Li, N. Chen, and G. H. Situ, "Deep-learning-based ghost imaging," Sci. Rep. **7**(1), 17865 (2017).
13. H. K. Hu, S. Sun, H. Z. Lin, L. Jiang, and W. T. Liu, "Denoising ghost imaging under a small sampling rate via deep learning for tracking and imaging moving objects," Opt. Express **28**(25), 37284 (2020).
14. Z. J. Li, Q. Zhao, and W. L. Gong, "Distorted point spread function and image reconstruction for ghost imaging," Optics and Lasers in Engineering **139**, 106486 (2021).
15. W. L. Gong, "Sub-Nyquist ghost imaging by optimizing point spread function," Opt. Express **29**(11), 17591–17601 (2021).
16. P. L. Zhang, W. L. Gong, X. Shen, D. J. Huang, and S. S. Han, "Improving resolution by the second-order correlation of light fields," Opt. Lett. **34**(8), 1222–1224 (2009).
17. F. R. S. Lord Rayleigh, "Investigations in optics, with special reference to the spectroscope," Philos. Mag. **8**(49), 261–274 (1879).
18. A. J. den Dekker and A. van den Bos, "Resolution: a survey," J. Opt. Soc. Am. A **14**(3), 547–557 (1997).
19. F. Ferri, D. Magatti, A. Gatti, M. Bache, E. Brambilla, and L. A. Lugiato, "High-resolution ghost image and ghost diffraction experiments with thermal light," Phys. Rev. Lett. **94**(18), 183602 (2005).
20. F. Ferri, D. Magatti, V. G. Sala, and A. Gatti, "Longitudinal coherence in thermal ghost imaging," Appl. Phys. Lett. **92**(26), 261109 (2008).
21. W. L. Gong, P. L. Zhang, X. Shen, and S. S. Han, "Ghost 'pinhole' imaging in Fraunhofer region," Appl. Phys. Lett. **95**(7), 071110 (2009).
22. B. I. Erkmen and J. H. Shapiro, "Ghost imaging: from quantum to classical to computational," Adv. Opt. Photonics **2**(4), 405–450 (2010).
23. P. Zerom, Z. M. Shi, M. N. O'Sullivan, K. W. Chan, M. Krogstad, J. H. Shapiro, and R. W. Boyd, "Thermal ghost imaging with averaged speckle patterns," Phys. Rev. A **86**(6), 063817 (2012).
24. W. L. Gong and S. S. Han, "High-resolution far-field ghost imaging via sparsity constraint," Sci. Rep. **5**(1), 9280 (2015).
25. E. F. Zhang, W. T. Liu, and P. X. Chen, "Ghost imaging with non-negative exponential speckle patterns," J. Opt. **17**(8), 085602 (2015).
26. K. Kuplicki and K. W. C. Chan, "High-order ghost imaging using non-Rayleigh speckle sources," Opt. Express **24**(23), 26766–26776 (2016).
27. Z. Sun, F. Tuitje, and C. Spielmann, "Toward high contrast and high-resolution microscopic ghost imaging," Opt. Express **27**(23), 33652–33662 (2019).
28. W. Tan, X. W. Huang, T. Jiang, S. Q. Nan, Q. Fu, X. P. F. Zou, Y. F. Bai, and X. Q. Fu, "Critical resolution in ghost imaging system with pseudo-thermal light," Results Phys. **32**, 105104 (2022).
29. J. W. Goodman, *Speckle Phenomena in Optics: Theory and Applications* (Roberts, 2007).
30. W. Zhang and M. G. Kuzyk, "Effect of a thin Kerr medium on a Laguerre-Gaussian beam," Appl. Phys. Lett. **89**(10), 101103 (2006).
31. J. Collins and A. Stuart, "Len-system diffraction integral written in terms of matrix optics," J. Opt. Soc. Am. A **60**(9), 1168–1177 (1970).
32. D. Magatti, A. Gatti, and F. Ferri, "Three-dimensional coherence of light speckles: Experiment," Phys. Rev. A **79**(5), 053831 (2009).
33. K. W. C. Chan, M. N. O'Sullivan, and R. W. Boyd, "Optimization of thermal ghost imaging: high-order correlations vs. background subtraction," Opt. Express **18**(6), 5562–5573 (2010).
34. W. Tan, X. W. Huang, S. Q. Nan, Y. F. Bai, and X. Q. Fu, "Effect of the collection range of a bucket detector on ghost imaging through turbulent atmosphere," J. Opt. Soc. Am. A **36**(7), 1261–1266 (2019).
35. X. W. Huang, S. Q. Nan, W. Tan, Y. F. Bai, and X. Q. Fu, "Ghost imaging for detecting trembling with random temporal changing," Opt. Lett. **45**(6), 1354–1357 (2020).
36. C. H. Liang, G. F. Wu, F. Wang, W. Li, Y. J. Cai, and S. A. Ponomarenko, "Overcoming the classical Rayleigh diffraction limit by controlling two-point correlations of partially coherent light sources," Opt. Express **25**(23), 28352–28362 (2017).